Availableonlineathttp://www.journalcra.com.com

International Journal of Current Research

Vol. 17, Issue, 02, pp.31989-31995, February, 2025
DOI: https://doi.org/10.24941/ijcr.48448.02.2025

INTERNATIONAL JOURNAL OF CURRENT

ISSN: 0975-833X

RESEARCHARTICLE

LEFT VENTRICULAR TWISTING MODEL TO SIMULATE LEFT VENTRICULAR CONTRACTION AND PRESSURE INCREASE DURING ISOVOLUMIC CONTRACTION

***[1]Dhanjoo N. Ghista, [2]Liu Li, [3]Ru San Tan and[4]Vidya K. Sudarshan**

[1]University 2020 Foundation, San Jose, California, USA; [2]OceanSTAR Marine & Offshore Pte, Ltd., Singapore
[3]Department of Cardiology, National Heart Centre, Singapore 168752; [4]College of Computing and Data Science, Nanyang Technological University, Singapore

ARTICLE INFO

Article History:
Received 30th September, 2024
Received in revised form
15th November, 2024
Accepted 26th December, 2024
Published online 27th February, 2025

Key words:
Left Ventricular Contraction,
Left Ventricular Twisting,
Myocardial Fibers' Orientation,
Left Ventricular Contractility.

**Corresponding author:*
Vidya K. Sudarshan

ABSTRACT

Background: It is well known that the tremendous internal pressure build-up in the left ventricle (LV) cavity during isovolumic contraction is due to the contraction of the spirally woven myocardial fibers.
Methodology and Results: In this chapter, a biomechanics model of the left-ventricle (LV) is developed to investigate the mechanism of LV pressure generation during isovolumic contraction. The LV is modeled as a fluid-filled thick-walled cylinder (with both ends closed) to simulate isovolumic contraction. We have shown that the tremendous internal cavity pressure build-up during isovolumic contraction is contributed by active torsion and compression caused by the contraction of the spirally wound myocardial fibers. We have matched the magnitude of the principal compressive stresses to the isometric myocardial fiber stresses, and then determined their orientation required for the LV model to generate the monitored pressure. In this process, we have also determined the constitutive property of the myocardial fibers, as well as magnitude of the stress generated in them and their equivalent orientation corresponding to the magnitude and direction of the principal stresses.
Conclusion: The results indicate that both myocardial fiber stresses and orientations (as given by the principal stresses) vary during the isovolumic contraction phase. The most significant aspect of our work is that LV twisting is a vital mechanism for the high intra-LV cavity pressure build-up during isovolumic contraction. Additionally, we have shown that the fiber orientation (based on the principal stress' directions) conforms to the values monitored in literature. Thus, we could conceivably employ the twist angle (derived noninvasively by MRI Tagging) as an LV contractility parameter.
Significance: Using this LV Twisting model, we can determine the myocardial fibers' orientation. This can have an important bearing on the capacity of the LV to generate adequate pressure during isovolumic contraction. By applying our model to patients, we can determine the ranges of fiber orientation in normal LVs and infarcted LVs. Based thereon, this model can also be used to diagnose impaired LVs. Further, the value of the compression principal stress and its orientation can be adopted as a measure of LV contractility.

Citation: Dhanjoo N. Ghista, Liu Li, Ru San Tan and Vidya K. Sudarshan,2025. *"***Left ventricular twisting model to simulate left ventricular contraction and pressure increase during isovolumic contraction***". International Journal of Current Research, 17, (02), 31989-31995.*

1. Introduction and Scope

Dynamics of the Left Ventricle during isovolumic contraction: It is interesting to study the dynamics of the left ventricle (LV) during isovolumic contraction, in order to determine how the LV develops an order-of-magnitude increase in pressure (of 60-100 mm Hg) in such a short period of time (approximately 0.05 – 0.06 secs) (Ingram, 1986; Fung, 1997). In this article, a biomechanics model of the LV is developed to investigate the mechanism of LV pressure generation during isovolumic contraction. The LV is modeled as a fluid-filled thick-walled cylinder (with both ends closed) to simulate isovolumic contraction. The upper end of the LV model is constrained in the long-axis direction to represent the suspension of the left ventricle by the aorta at the base. A schematic of the myocardial fiber orientation within the LV wall is depicted in Figure 1-A.

Contraction of the helically wound myocardial fibers creates torsion and compression of the LV, to in turn generate pressure within it. Herein, we are carrying out an inverse analysis, by determining the stress-state in the LV model to generate the pressure.

From the stress-state, we determine the (i) principal stresses and the associated myocardial fibers stresses, along with the compressive principal stress and its orientation, and (ii) the equivalent compression force and torsion applied to the LV (due to myocardial fibers' contraction) to generate pressure within it.

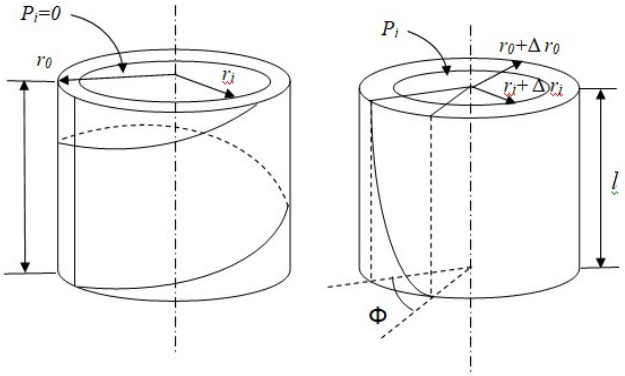

Figure 1-A. Schematic of the myocardial fiber orientation for the cylindrical LV model

In Figure 1-B, we depict this LV model cylinder wall to be composed of myocardial fiber units, helically wrapped within the LV cylindrical wall. Half of these fibers are wrapped in a clockwise fashion, and the other half of fibers are wrapped in counterclockwise fashion. The biomechanical model ultra-structure of each fiber is the myocardial structural unit (MSU), as depicted in Figure 2.

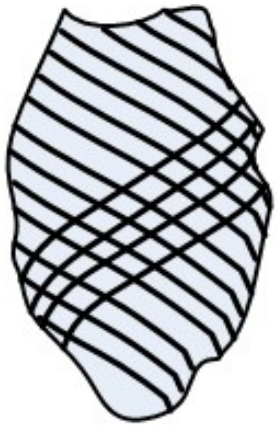

Figure 1-B. Schematic of LV myocardial fibers helically wrapped within the LV model wall.

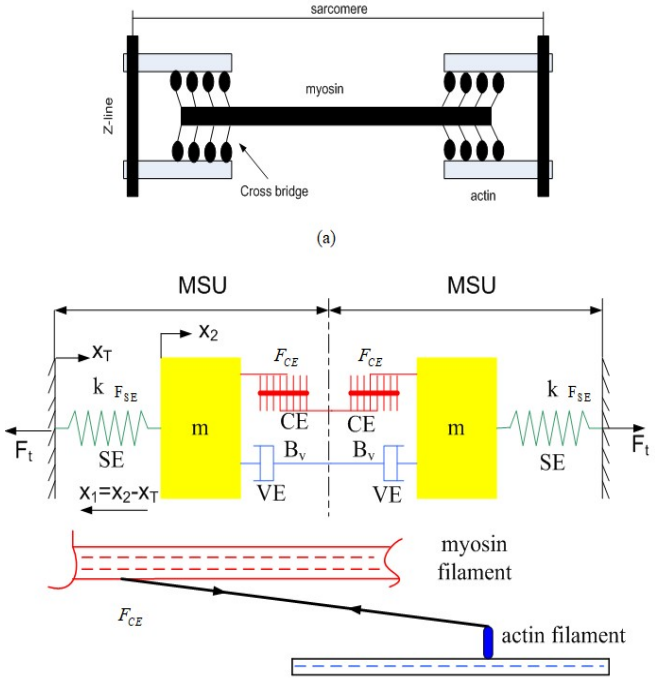

Figure 2. (a) The actin and myosin filaments constituting the contractile components of the myocardial fibril; (b) Myocardial fibril model composed of two symmetrical myocardial structural units (MSUs), which are mirror images of each other. Each MSU is composed of (i) an effective mass (m) that is accelerated; (ii) connective-tissue series element having parameter k (elastic modulus of the series element) and the force F_{SE}; (iii) the contractile element (CE), which generates contractile force FCE between the myosin(thick) and actin (thin) filaments; (iv) the parallel viscous element of the sarcolemma havingviscous damping parameter B v and force FVE. During ejection, the MSU x_T decreases, and during filling the MSU x_T increases. (This figure is adopted from our paper: Ghista DN, Zhong L, Ng EYK, Lim ST, Tan RS, Chua T, Systolic modeling of the left ventricle as a mechatronic system: determination of myocardial fiber's sarcomere contractile characteristics and new performance indices, Molecular & Cellular Biomechanics, 2(4):217-233, 2005).

2. LV cylindrical Model Geometry Development based on Data Collection: The LV data, derived from the cineventriculographic measurements hence consists of LV pressure, LV volume (V), LV wall thickness (h), and hence of LV myocardial volume (V_M). There from, we can determine the geometrical parameters of the LV cylindrical model, as defined in Figure 1-A.

For our analysis, we start with the data of V = 1.367 x 10^2 ml, VM = 185 ml, ri = *2.03* cm,h = 1.085 cm, ro= 3.12 cm, l = 10.53 cm, and incremental pressure Δp = 22mm Hg during the three stages of isovolumic contraction. The total twisting angle (Φ) of the left-ventricle during isovolumic phase is obtained from myocardial tagging based on MRI. Herein the total $\Phi \approx 2^\circ$, and hence we adopt $(2/3)^\circ$ as the average twist angle for each of the three periods of isovolumic contraction.

3. Modelling the Biomechanics of the LV during isovolumic contraction: In order to model the biomechanics of the LV during isovolumic contraction, we subject the model to longitudinal, radial, and circumferential deformations (derivable from the MRI LV geometries) at three instants during isovolumic contraction. These longitudinal, radial, and circumferential deformations correspond to the observed shortening, contraction, and twisting of the LV during the isovolumic contraction phase, caused by the contraction of the (helically wound) myocardial fibers.From these deformations, we determine the relevant strains in the LV wall, using strain-displacement relations. From the strains, we express the stresses in terms of the elastic moduli (E_z, E_r, E_θ and G), using stress-strain equations. Now we impose the boundary condition for wall radial stress on the inner surface of the LV, by equating it to the monitored incremental LV pressure. Since the radial stress $\sigma_r(r=r_i)$ is a function of the constitutive parameters (E_z, E_r, E_θ), we can also determine the best-fit values of these constitutive parameters, from the boundary conditions: $\sigma_{r,j}(R_i) = -p_j$, for j = 1, 2, 3 time instants.

Having determined the constitutive moduli, we then return back to calculate the stresses in terms of the monitored displacements. We next determine the principal stresses and their orientations, and postulate that the LV myocardial fibers are oriented along these principal directions. We then confirm that these derived fiber orientations are in the same range as the histologically derived fiber orientations. In this way, we are demonstrating that the tremendous rise in the intra-LV blood pressure during isovolumic contraction is due to the active twisting and compression caused by the generated principal stress, corresponding to the actively contracting spirally oriented myocardial fibers within the LV wall. Hence, indirectly, we are demonstrating the phenomenon of LV shortening and twisting in the process of intra-LV pressure increase during isovolumic contraction.

4. Bioengineering Formulation: The LV deformation during the short period of isovolumic contraction phase is modeled by using three available time frames. It is thus reasonable to assume that the displacement of the myocardial points to be relatively small within each time step, and hence the left ventricular myocardial wall can be modeled as a linear elastic material within this short time interval. We further assume the material of the left ventricular wall to be incompressible [Chaudhry, 1996].

The left ventricle (LV) at end-diastole is assumed to be in a relaxed state. The activation of its spirally-oriented myocardial fibers and the associated LV deformations during isovolumic contraction, results in the application of equivalent torsion and compression (ΔM_T and ΔF) to its bottom surface (as illustrated in Figure 3)during isovolumic contraction. We solve this problem in an inverse fashion, by utilizing the monitored pressure increment $\Delta P(t)$ from the clinical data, to compute the instantaneous volume increment $\Delta V(t)$ from the bulk modulus $(K)$of the blood. From $\Delta V(t)$, we determine the associated displacements, and hence the strains and stresses in terms of

the constitutive parameters. We then equate the radial stress on the inner surface of the LV to the internal pressure *P(t)*, and have the axial stress equilibrate the pressure on the endplate, and thereby solve for the constitutive parameters. We then return to the stress state, and determine the resultant equivalent ΔM_T and ΔF applied to the LV cylindrical model, as a result of the contraction of the spirally-wound myocardial fibers.

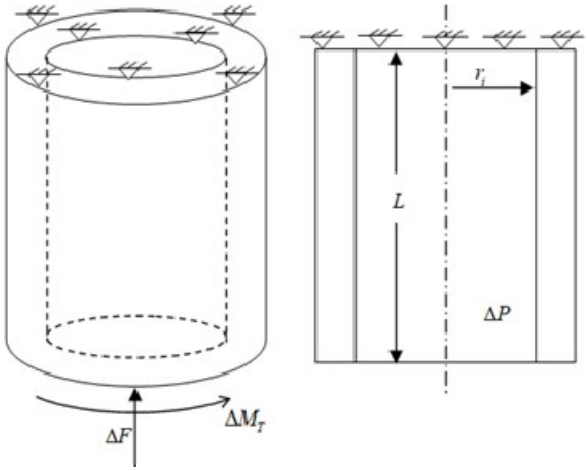

Figure 3. Geometry of the fluid-filled LV model. As a result of the axial, radial, and circumferential deformations generated within the LV cylindrical model(due to the activation of the spirally-wound myocardial fibers) compression and torque ΔF and ΔM_T are generated, and act on the suspended surface of the cylindrical model. Alternatively, we can take ΔF and ΔM_T as equivalent force and torque being applied to the bottom surface to produce these deformations.

We now provide the governing equations of linear elasticity in cylindrical polar coordinates.

The equations of equilibrium (without body forces) are:

$$\frac{1}{r}\frac{\partial}{\partial r}\left(r\sigma_{rr}\right)+\frac{1}{r}\frac{\partial\sigma_{r\theta}}{\partial\theta}+\frac{\partial\sigma_{rz}}{\partial z}-\frac{1}{r}\sigma_{\theta\theta}=0 \quad (1\text{-a})$$

$$\frac{1}{r}\frac{\partial\sigma_{\theta\theta}}{\partial\theta}+\frac{1}{r}\frac{\partial}{\partial r}\left(r\sigma_{r\theta}\right)+\frac{\partial\sigma_{z\theta}}{\partial z}+\frac{1}{r}\sigma_{r\theta}=0 \quad (1\text{-b})$$

$$\frac{\partial\sigma_{zz}}{\partial z}+\frac{1}{r}\frac{\partial}{\partial r}\left(r\sigma_{rz}\right)+\frac{1}{r}\frac{\partial\sigma_{z\theta}}{\partial\theta}=0 \quad (1\text{-c})$$

where *r, θ and z* represent the radial, circumferential and long-axis direction respectively, and σ_{ij} are the corresponding LV wall stresses.

The stress-strain relations are:

$$\varepsilon_{rr}=\frac{1}{E_r}(\sigma_{rr}-\nu\sigma_{\theta\theta}-\nu\sigma_{zz}) \quad (2\text{-a})$$

$$\varepsilon_{\theta\theta}=\frac{1}{E_\theta}(-\nu\sigma_{rr}+\sigma_{\theta\theta}-\nu\sigma_{zz}) \quad (2\text{-b})$$

$$\varepsilon_{zz}=\frac{1}{E_z}(-\nu\sigma_{rr}-\nu\sigma_{\theta\theta}+\sigma_{zz}) \quad (2\text{-c})$$

$$\varepsilon_{z\theta}=\frac{\sigma_{z\theta}}{2G_{z\theta}} \quad (2\text{-d})$$

$$\varepsilon_{r\theta}=\frac{\sigma_{r\theta}}{2G_{r\theta}} \quad (2\text{-e})$$

$$\varepsilon_{rz}=\frac{\sigma_{rz}}{2G_{rz}} \quad (2\text{-f})$$

where ε_{ij} are the LV wall strains in the different directions, E_{ij} and G_{ij} are the elastic modulus and shear modulus in the corresponding directions respectively, while *v* is the Poisson's ratio of the material.

The strain-displacement relations are:

$$\varepsilon_{rr}=\frac{\partial u_r}{\partial r} \quad (3\text{-a})$$

$$\varepsilon_{\theta\theta}=\frac{1}{r}\frac{\partial u_\theta}{\partial\theta}+\frac{u_r}{r} \quad (3\text{-b})$$

$$\varepsilon_{zz}=\frac{\partial u_z}{\partial z} \quad (3\text{-c})$$

$$\varepsilon_{rz}=\frac{1}{2}\left(\frac{\partial u_r}{\partial z}+\frac{\partial u_z}{\partial r}\right) \quad (3\text{-d})$$

$$\varepsilon_{r\theta}=\frac{1}{2}\left(\frac{1}{r}\frac{\partial u_r}{\partial\theta}+\frac{\partial u_\theta}{\partial r}-\frac{u_\theta}{r}\right) \quad (3\text{-e})$$

$$\varepsilon_{\theta z}=\frac{1}{2}\left(\frac{\partial u_\theta}{\partial z}+\frac{1}{r}\frac{\partial u_z}{\partial\theta}\right) \quad (3\text{-f})$$

Because of the axially symmetric deformation, the components of the stress-tensor in cylindrical coordinates can be expressed as functions of r alone. Then, the equations of equilibrium can be written as:

$$\frac{\mathrm{d}\sigma_{rr}}{\mathrm{d}r}+\frac{\sigma_{rr}-\sigma_{\theta\theta}}{r}=0 \quad (4\text{-a})$$

$$\frac{\mathrm{d}\sigma_{r\theta}}{\mathrm{d}r}+\frac{2\sigma_{r\theta}}{r}=0 \quad (4\text{-b})$$

$$\frac{\mathrm{d}\sigma_{rz}}{\mathrm{d}r}+\frac{\sigma_{rz}}{r}=0 \quad (4\text{-c})$$

Similarly, because of the axially symmetric deformation, the shear strains $\varepsilon_{r\theta}$ and ε_{rz} are taken to be zero.

Now, the boundary conditions on the outer and inner surfaces as well as top and bottom surfaces of the LV cylindrical model are given as:

$$\sigma_{rr}\left(r=r_o\right)=0 \quad (5\text{-a})$$

$$\sigma_{rr}\left(r=r_i\right)=-p \quad (5\text{-b})$$

$$\sigma_z\pi\left(r_o^2-r_i^2\right)=p\left(\pi r_i^2\right) \quad (5\text{-c})$$

where *p* represents the monitor able intra-ventricular pressure developed by LV contraction.

5.Satisfying Boundary Conditions and Determination of the myocardial constitutive parameters

i) We obtain the blood pressure increment ΔP from the clinical data during the isovolumic contraction phase. The total increment in blood pressure during the short period of time of isovolumic contraction is recorded as 66 mmHg. The pressure increase ΔP is recorded over three time-periods (of 0.02 secs duration). Hence, for each instant, ΔP_j is adopted to be 22 mmHg.

ii) By taking the blood bulk modulus K = 2.10 x 10^9, we can compute the volume strain ($\Delta V/V$) in the LV chamber volume

$$\varepsilon_{v_j} = -\Delta P_j / K \cdot$$

The pressure is obtained by catheterization for different time intervals. The LV volume (V), myocardial volume (VM), and wall thickness (h) are measured by ventriculography at the beginning of isovolumic contraction.

iii) For each computed value of ΔV, we obtain the *change-of-length* (Δl) and the *decrease of the internal radius* (Δr_i) by assuming that the ratio of the length change is p times of the decrease of inner radius during isovolumic contraction. Hence,

$$\Delta l = (p)kl\,,\ \Delta r_i = kr_i$$
$$(1+pk)(1-k)^2 - 1 = -\Delta P/K\ ,\text{LV chamber volume strain } (\Delta V/V) \tag{6}$$

wherein l and r_i are the original length and internal radius of the LV model, respectively. Due to the incompressibility of the LV wall material, we can evaluate the change in outer radius as:

$$\Delta r_o = \sqrt{l(r_o^2 - r_i^2)/(l+\Delta l) + (r_i^2 - \Delta r_i^2)} - r_o \tag{7}$$

iv) Now, we can evaluate the radial displacement **(u_r)** at any point within the LV wall by using the following equation: (assuming the strain changed linearly through the LV wall):

$$u_r = \frac{\Delta r_i}{r_i} r + \frac{r_i \Delta r_o - r_o \Delta r_i}{r_o r_i (r_o - r_i)} (r^2 - r_i r)\ , \tag{8-a}$$

$$u_\theta = z\frac{\Phi}{l}, \tag{8-b}$$

$$u_z = \frac{\Delta l}{l} z\ , \tag{8-b}$$

where Φ is twisting angle and Δl is the shortening of length.

v) We can then calculate the strain components from equations (3) and (8) in the different directions as

$$\varepsilon_{rr} = \frac{\Delta r_i}{r_i} + \frac{r_i \Delta r_o - r_o \Delta r_i}{r_o r_i (r_o - r_i)} (2r - r_i) \tag{9-a}$$

$$\varepsilon_{\theta\theta} = \frac{\Delta r_i}{r_i} + \frac{r_i \Delta r_o - r_o \Delta r_i}{r_o r_i (r_o - r_i)} (r - r_i) \tag{9-b}$$

$$\varepsilon_{zz} = \frac{\Delta l}{l}\ ; \tag{9-c}$$

$$\varepsilon_{\theta z} = \frac{r\Phi}{2l} \tag{9-d}$$

vi) We can now express the stress components in terms of the displacements and constitutive properties, by employing equations (2 a-d) and equation (9 a-d), as follows

$$\sigma_{rr} = \frac{E_r(1-\nu)}{(1+\nu)(1-2\nu)}\left(\frac{\Delta r_i}{r_i} + \frac{r_i\Delta r_o - r_o\Delta r_i}{r_o r_i (r_o - r_i)}(2r - r_i)\right) + \frac{\nu}{(1+\nu)(1-2\nu)}\left(E_\theta\left(\frac{\Delta r_i}{r_i} + \frac{r_i\Delta r_o - r_o\Delta r_i}{r_o r_i (r_o - r_i)}(r - r_i)\right) + E_z\frac{\Delta z}{l}\right) \tag{10-a}$$

$$\sigma_{\theta\theta} = \frac{E_r\nu}{(1+\nu)(1-2\nu)}\left(\frac{\Delta r_i}{r_i} + \frac{r_i\Delta r_o - r_o\Delta r_i}{r_o r_i (r_o - r_i)}(2r - r_i)\right) + \frac{1}{(1+\nu)(1-2\nu)}\left(E_\theta(1-\nu)\left(\frac{\Delta r_i}{r_i} + \frac{r_i\Delta r_o - r_o\Delta r_i}{r_o r_i (r_o - r_i)}(r - r_i)\right) + E_z\nu\frac{\Delta z}{l}\right) \tag{10-b}$$

$$\sigma_z = \frac{E_r\nu}{(1+\nu)(1-2\nu)}\left(\frac{\Delta r_i}{r_i} + \frac{r_i\Delta r_o - r_o\Delta r_i}{r_o r_i (r_o - r_i)}(2r - r_i)\right) + \frac{1}{(1+\nu)(1-2\nu)}\left(E_\theta\nu\left(\frac{\Delta r_i}{r_i} + \frac{r_i\Delta r_o - r_o\Delta r_i}{r_o r_i (r_o - r_i)}(r - r_i)\right) + E_z(1-\nu)\frac{\Delta z}{l}\right) \tag{10-c}$$

$$\sigma_{\theta z} = G_{\theta z}\frac{r\Phi}{l} \tag{10-d}$$

vii) By integration of equation (4-a) and substituting for σ_{rr} and $\sigma_{\theta\theta}$ from equations (10-a) and (10-b), we get:

$$\begin{aligned}\sigma_{rr}(r) &= \int_r^{r_o}(\sigma_{rr} - \sigma_{\theta\theta})\frac{dr}{r}\\ &= \int_r^{r_o}\frac{1}{(1+\nu)}\left(E_r\left(\frac{\Delta r_i}{r_i} + \frac{r_i\Delta r_o - r_o\Delta r_i}{r_o r_i (r_o - r_i)}(2r - r_i)\right) - E_\theta\left(\frac{\Delta r_i}{r_i} + \frac{r_i\Delta r_o - r_o\Delta r_i}{r_o r_i (r_o - r_i)}(r - r_i)\right)\right)\frac{dr}{r}\\ &= \frac{E_r}{(1+\nu)}\left(\frac{\Delta r_i}{r_i}\ln r + \frac{r_i\Delta r_o - r_o\Delta r_i}{r_o r_i (r_o - r_i)}(2r - r_i\ln r)\right)\Bigg|_r^{r_o}\\ &\quad - \frac{E_\theta}{(1+\nu)}\left(\frac{\Delta r_i}{r_i}\ln r + \frac{r_i\Delta r_o - r_o\Delta r_i}{r_o r_i (r_o - r_i)}(r - r\ln r)\right)\Bigg|_r^{r_o}\end{aligned} \tag{11}$$

Now, by imposing the boundary conditions (5), we obtain:

$$\begin{aligned}p_i(\Delta t_i) &= -\int_{r_i}^{r_o}(\sigma_{rr} - \sigma_{\theta\theta})\frac{dr}{r}\\ &= \frac{E_r}{(1+\nu)}\left(\frac{\Delta r_i}{r_i}\ln r + \frac{r_i\Delta r_o - r_o\Delta r_i}{r_o r_i (r_o - r_i)}(2r - r_i\ln r)\right)\Bigg|_{r_i}^{r_o}\\ &\quad - \frac{E_\theta}{(1+\nu)}\left(\frac{\Delta r_i}{r_i}\ln r + \frac{r_i\Delta r_o - r_o\Delta r_i}{r_o r_i (r_o - r_i)}(r - r\ln r)\right)\Bigg|_{r_i}^{r_o}\end{aligned} \tag{12}$$

Then, by equalizing this intra-ventricular pressure p expression to the monitored value of incremental pressure 22 mmHg, we can compute the material property (E_r, E_θ, E_z) by solving equations (12), (5-a,b,c), and (10).

viii) The value of parameter p is determined by guaranteeing the values of the material properties (E_r, E_θ, E_z) to be positive. Then the parameter p is calculated as 1.75.

ix) The shear stress $\sigma_{\theta z}$ can be expressed as a functions of the principal orientation

$$\sigma_{\theta z} = \tan(2\Phi)\,(\sigma_{\theta\theta} - \sigma_{zz})/2 \qquad (13)$$

and the principal stresses can also be expressed as functions of principal orientation:

$$\sigma_{1,2} = \frac{(\sigma_{\theta\theta} + \sigma_{zz})}{2} \pm \sqrt{(\frac{\sigma_{\theta\theta} - \sigma_{zz}}{2})^2 + (\sigma_{\theta z})^2} \qquad (14)$$

x)Figure 4 displays active fiber tension predicted by different models at different ranges of sarcomere length. The active fiber tension is shown to increase linearly during isovolumic contraction. It can be seen that the maximum value of fiber tension is 135.7 Kpa, corresponding to the principal compressive stress, achieved at the longest sarcomere length. Hence, we calculated the shear stresses and compressive principal compressive stress according to different values of the fiber angle. The discrepancy between computed principal stress and the presumed fiber tension is shown in Figure 5. We can read the optimal fiber angle at different instants as given by 36.2^0, 35.3^0, 34.4^0.

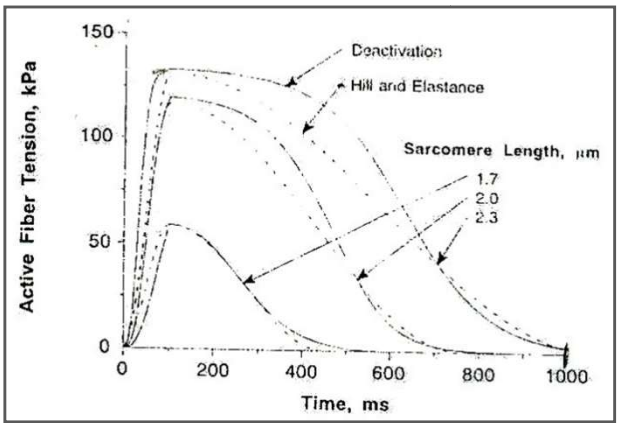

Figure 4. Active Fiber tension (Isometric twitches) predicted by the different models at a range of sarcomere length.

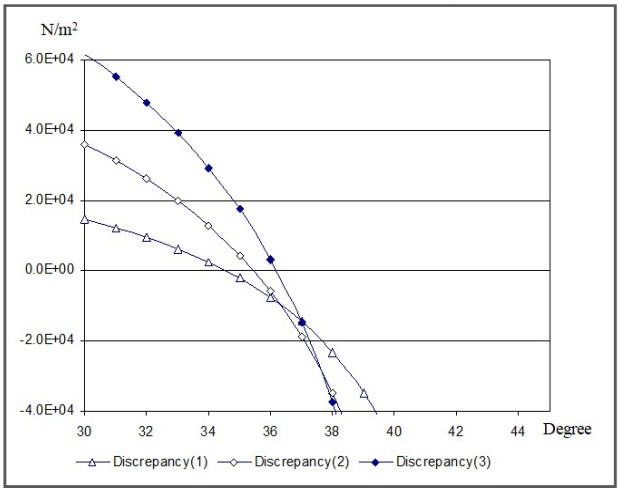

Figure 5. Discrepancy of the calculated results and the presumed fiber tension with fiber angle.

xi) The total twisting angle (Φ) of the left-ventricle during isovolumic phase is obtained from myocardial tagging based on MRI (Nagel *et al*., 2000;Aelen, 1997). Herein the total $\Phi \approx 2^\circ$, and hence we adopt $(2/3)^\circ$ as the average twist angle for each of the three periods of isovolumic contraction. Hence, we can calculate the Shear modulus from the equation (10-d). xii) Till now we have obtained the stresses and the corresponding principal stresses. We can now determine the internally generated equivalent axial force F and the torsional couple M_T associated with the deformations generated in the LV by the spirally oriented myocardial fiber activation.

The expressions for ΔF and ΔM_T are obtained as:

$$\Delta F = 2\pi\int_{r_i}^{r_o} \sigma_{zz} r\,dr = \frac{2\pi E_r \nu}{(1+\nu)(1-2\nu)}\left(\frac{\Delta r_i r^2}{2r_i} + \frac{r_i\Delta r_o - r_o\Delta r_i}{r_o r_i (r_o - r_i)}\left(\frac{2r^3}{3} - \frac{r_i r^2}{2}\right)\right)\Bigg|_{r_i}^{r_o} + \frac{2\pi}{(1+\nu)(1-2\nu)}\left(E_\theta \nu\left(\frac{\Delta r_i r^2}{2r_i} + \frac{r_i\Delta r_o - r_o\Delta r_i}{r_o r_i (r_o - r_i)}\left(\frac{r^2}{3} - \frac{r_i r^2}{2}\right)\right) + E_z(1-\nu^2)\frac{\Delta z r^2}{2l}\right)\Bigg|_{r_i}^{r_o} \qquad (15)$$

$$\Delta M_T = 2\pi\int_{r_i}^{r_o} \sigma_{\theta z} r^2\,dr = \frac{\pi G_{\theta z}\Phi r^4}{2l}\Bigg|_{r_i}^{r_o} \qquad (16)$$

6. Results

The variations of the equivalent activated force and torque during the isovolumic phase are calculated and depicted in Figure 6 and Figure 7, respectively. In other words, by means of this model, we have demonstrated that the tremendous increase of the LV cavity pressure is caused by the internally generated torsional and axial forces during isovolumic contraction phase (in turn due to the contraction of the helically wound myocardial fibers).

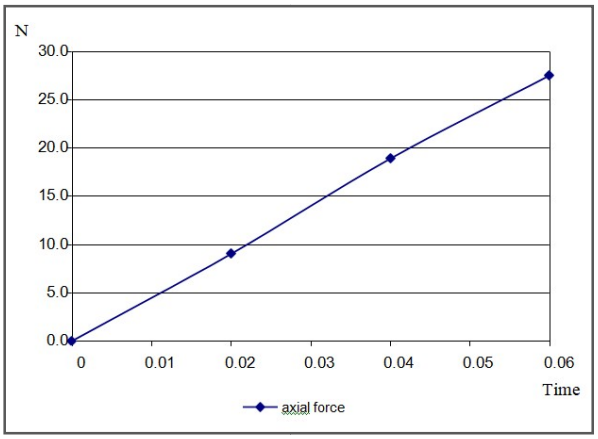

Figure 6. Variationoftheactivatedaxialforceduringisovolumic contraction phase.

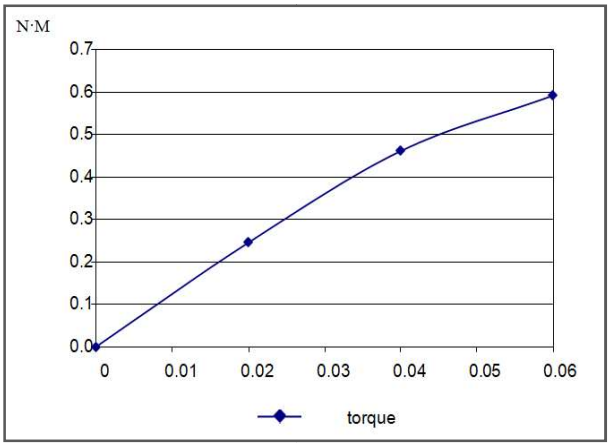

Figure 7. Variation of the activated torque during isovolumic contraction phase.

The variations of the stress components ($\sigma_{rr}, \sigma_{\theta z}, \sigma_{\theta\theta}, \sigma_{zz}$) during the isovolumic contraction phase are shown in Figure 8. It is seen that the axial and shear stresses induced are much larger than the circumferential stress and radial stress. The variations of principal stresses during isovolumic phase are depicted in Figure 9. It can be noted that the compressive principal stress is almost twice the value of the tensile principal stress, which is expected in the LV isovolumic

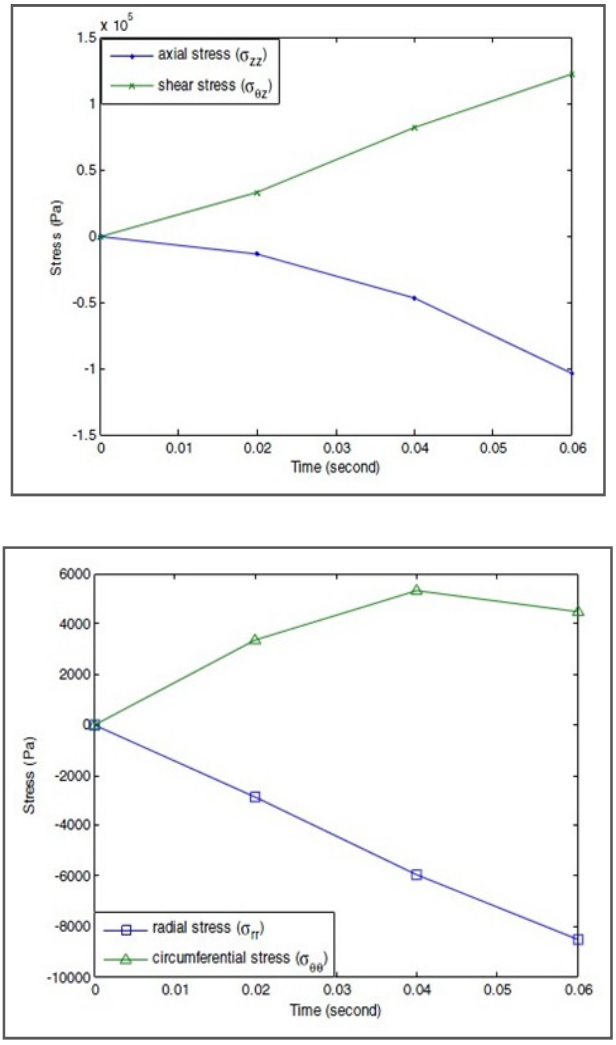

Figure 8. Variations of activated Axial stress (σ_{zz}), Shear stress ($\sigma_{\theta z}$), Radial stress (σ_{rr}), and Circumferential Stress ($\sigma_{\theta\theta}$) as functions of time during the Isovolumic Contraction phase

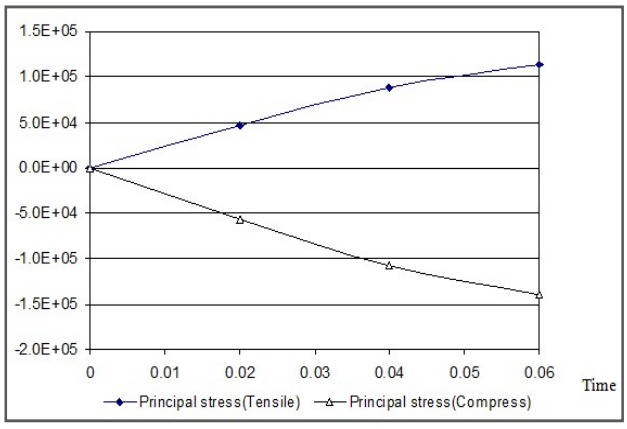

Figure 9. Variation of principal stresses generated during isovolumic contraction phase

contraction phenomenon. At the end of the isovolumic phase, the magnitude of the principal stress is around 1.375×10^5 Pa , which is in good agreement with the isometric tension achieved under maximal activation (Guccione, 1993). The variation of the fiber angle is illustrated in Figure 10. It is noted that both the principal stresses and the corresponding fiber angle are observed to vary throughout the isovolumic contraction phase. We can now adopt the principal stress directions to correspond to the myocardial fiber orientation, as shown in Figure 10. From Figure 10, we can note that the principal stress angle and hence the myocardial fiber orientation varies from 36.2 degrees at the start to 34.4 degrees at the end of the isovolumic phase, which corresponds to the range of the values reported by Streeter and co-workers (Streeter, 1979; Streeter, 1973; Streeter, 1978; Streeter, 1969). Also, it is expected that as the myocardial fibers contract, the fiber angle should decrease, which is as per our results. It is noteworthy that we have been able to determine the fiber orientation (corresponding to the principal stress orientation) from the LV deformation data. This may be deemed to be an important finding of our work. What we have shown is that from Δp and LV deformation, we can determine the fiber stress and fiber angle, which are important intrinsic properties of the LV myocardial structures. The fiber angle may be deemed to be a decisive property of the LV, which governs its contractile state and the generation of pressure within it (Figure 11). However, this requires determination of LV internal pressure (by catheterization) and LV deformation (by MRI imaging), both of which procedures need to be carried out separately.

TheLV twist which also has an important bearing on LV pressure generation (and which be determined from MRI imaging data) can emerge (based on this study) as a noninvasively determinable contractile index. Finally, Figure 12 depicts the calculated values of the elastic moduli.

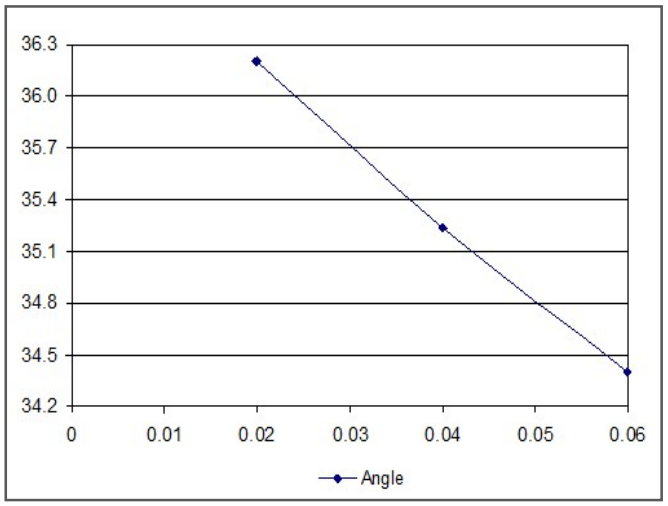

Figure 10. Variation of the fiber angle from 36.2 degrees at the start to 34.4 degrees at the end of the isovolumicphase

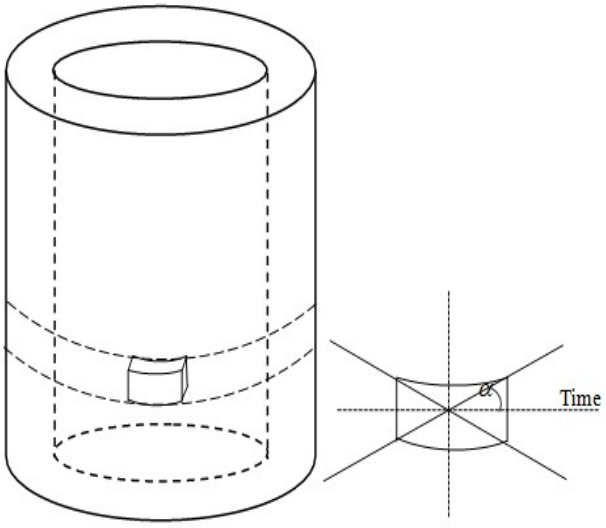

Figure11.Schematics of the orientation of the principal stresses, corresponding to the orientation of the myocardial fibers.

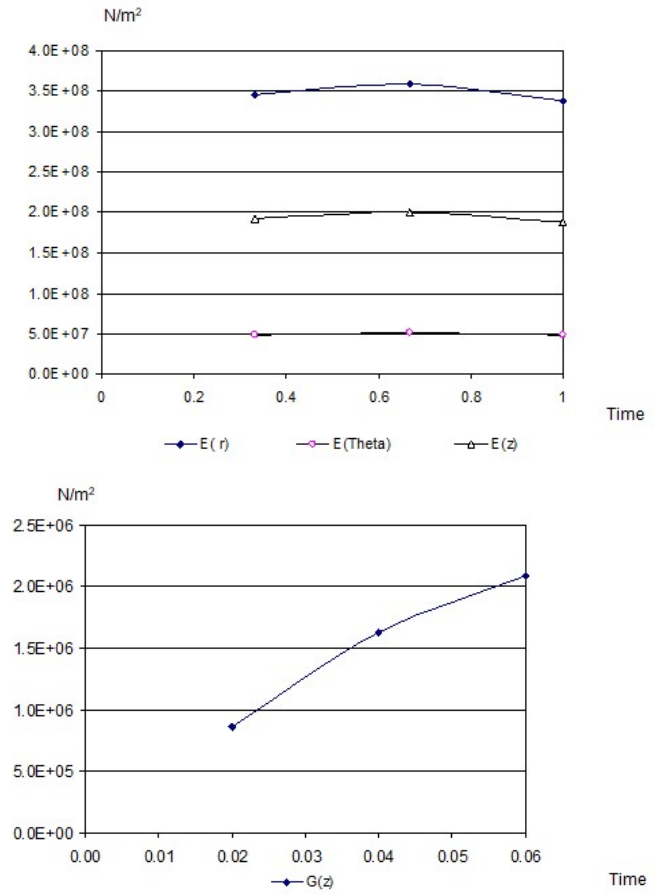

Figure 12. The calculated elastic moduli of the LV during isovolumic contraction phase

7. Discussion

From our results, it is apparent that the huge LV cavity pressure rise during isovolumic phase is largely due to torsion and compression generated in the LV wall by the contraction of the helically wound myocardial fibers. We are also associating the principal stresses to the myocardial fiber stresses and the principal direction to the myocardial fiber orientation. We can hence perceive that the LV torsion (associated with fiber shortening) is the primary mechanism involved in generating the high intra-LV cavity pressure build-up during isovolumic contraction, which is in good conformity with the investigations made by the previous researchers (MacGowan, 1996; Bovendeerd, 1992).

Our LV biomechanics model can be deemed to simulate isovolumic contraction, to evaluate the stresses and strains in the LV myocardium by using elasticity theory. In addition, our model has enabled determination of the myocardial fiber orientation and the fiber stresses corresponding to the principal stresses associated with the monitored deformation and the intra-LV pressure (Bovendeerd, 1992). Hence, we can employ the principal stress orientation and the principal stress value to constitute a new intrinsic measure of LV contractility.

Additionally, we are able to determine the in-vivo constitutive parameters (E_r, E_θ, ν). Since measurement of the in-vivo constitutive properties of the LV myocardium is difficult, this too is a significant contribution. By studying a wide range of patients, we can determine (i) their fiber orientations, (ii) myocardial constitutive properties, (iii) equivalent torsion ΔM_T and axial force ΔF, (iv) and the contractile stresses along the fibers. All of these indices can be employed diagnostically to differentiate between healthy and poorly contracting LV(s). Even more significant is our being able to determine the orientations of the principal stresses and hence the fiber orientation. We could make an assertion that the intrinsic capacity of a patient's LV to twist and eject depends on the orientation of the LV myocardial fiber. Those patient LVs with low values of the fiber angle will need to exert a lot more contractile energy than LVs with higher fiber angle. Internally, we have shown that the monitored pressure is caused by the calculated principal stresses and orientation of calculated myocardial fiber stress along the orientation of the principal stress. Conversely, if we were to have myocardial fibers along (the orientation of the principal stresses), and if the tensile force in the myocardial was equal to the maximum genera table isometric tension, then the pressure generated in the LV would be equal to the monitored pressure.In other words, for the pressure generated (equal to the monitored value), with the myocardial fibers generating isometric tension values, they need to be oriented at the calculated values at each period of the isovolumic contraction.

8. References

Aelen, F. W. L, Arts, T, Snaders, D. G. M, Thelissen, G. R. P, Muijtjens, A. M. M., Prinzen, F. W., Reneman, R.S., Relation between torsion and cross-section area change in the human left ventricle. *J Biomechanics*. 1997; 30(3):207-12.

Bovendeerd, PHM, Arts T, Huyghe JM, van Campen DH, and Reneman RS. Dependence of local left ventricular wall mechanics on myocardial fiber orientation: a model study. *J Biomec.*1992;25:1129-40,.

Chaudhry, H. R., Bukiet, B., and Davis, A. M., Stresses and strains in the left ventricular wall approximated as a thick conical shell using large deformation theory, *J Biol Systems.*1996; 4(3):353-72.

Fung, Y. C., Biomechanics Circulation, Springler-Verlag, 1997.

Guccione, J. M., Waldman, L. K., McCulloch, A. D., Mechanics of active contraction in Cardiac muscle: Part II- Cylindrical models of the systolic left ventricle. Journal of Biomechanical Engineering. 1993, 115(2):82-90.

Ingram, D. and Bloch, R. F., Mathematical methods in medicine, John Wiley & Sons Ltd., 1986.

MacGowan GA, Burkhoff D, Rogers WJ et al. Effects of afterload on regional left ventricular torsion. *Cardiovasc Res.* 1996;31: 917-25.

Nagel, N, Stuber, M, Burkhard, B, fischer, S. E, Scheideggerm, M. B, Boesiger, P and Hess, O. M. Cardiac rotation and relaxation in patients with aortic valve stenosis. *European Heart Journal*. 2000, 21, 582-589.

Streeter, DD, and Hanna WT**.** Engineering mechanics for successive states in canine left ventricular myocardium. II. Fiber angle and sarcomere length. *Circ Res*. 1973;33: 656-64.

Streeter, DD, Powers WE, Ross MA, and Torrent-Guasp F. Three-dimensional fiber orientation in the mammalian left ventricular wall. In: *Cardiovascular System Dynamics*, edited by Baan H, Noordergraaf A, and Raines J.. Cambridge, MA: MIT Press, 1978.

Streeter, DD, Spotnitz HM, Patel DP, Ross J, and Sonnenblick EH. Fiber orientation in the canine left ventricle during diastole and systole. *Circ Res.* 1969;24: 339-47.

Streeter, DD., Gross morphology and fiber geometry of the heart. In: Handbook of Physiology. The Cardiovascular System. The Heart. Bethesda, MD: Am. Physiol. Soc, sect. 2, 1979; I: 61-112.

****